Supplementary Information for Coupling Effects on Access Resistance of In-Series Nanopores

Jacob Bair,[1] Thor Burkhardt,[1] Zachery Gottshall,[1] and Matthias Kuehne*[1]
*Department of Physics, Brown University, Providence, RI 02912, United States. *Email: kuehne@brown.edu*

S1. SOLUTION FOR A SINGLE LONG NANOCHANNEL

We consider the case of a single nanochannel of finite length, l_n, as shown in Fig. S1. The general solution to Laplace's equation for this geometry is given by Eq. (4) in the main text. The boundary conditions that must be satisfied take the same form as those for the case of a two pore system, but with l_c replaced with l_n and r_c replaced with r_n. Again, due to the symmetry of the system about a plane perpendicular to the z-axis which we define to be located at $z = 0$, we consider the solution only in the half space $z \leq 0$. We solve for the potential in each of the two compartments existing in the half-space separately, the lower exterior compartment and half of the nanochannel, and then match the solutions at $z = -l_\mathrm{n}/2$ to obtain the resistance. Making the relevant changes to the boundary conditions, we have, for the outer macroscopic compartment,

$$\phi_\mathrm{m}\left(r,\ -l_\mathrm{m} - \frac{l_\mathrm{n}}{2}\right) = \frac{\Delta V}{2} \tag{S1}$$

and

$$\left.\frac{\partial \phi_\mathrm{m}}{\partial r}\right|_{r=r_\mathrm{m}} = 0 \tag{S2}$$

We also have

$$\left.\frac{\partial \phi_\mathrm{m}}{\partial z}\right|_{z=-l_\mathrm{n}/2} = \begin{cases} -\rho_\mathrm{bulk} i\,(r) & 0 \leq r < r_\mathrm{n} \\ 0 & r_\mathrm{n} \leq r \leq r_\mathrm{m} \end{cases} \tag{S3}$$

and again assume the radial inverse square root current density given by Eq. (11) in the main text. From these conditions we obtain $k_{g,\mathrm{m}} = \beta_g / r_\mathrm{m}$, $B_\mathrm{m} = \rho_\mathrm{bulk} I / \pi r_\mathrm{m}^2$, and $A_\mathrm{m} = \Delta V/2 - \rho_\mathrm{bulk} I\,(2l_\mathrm{m} + l_\mathrm{n})\,/2\pi r_\mathrm{m}^2$, and

$$a_{g',\mathrm{m}} = -\frac{\rho_\mathrm{bulk} I \sin\left(\beta_{g'} r_\mathrm{n}/r_\mathrm{m}\right)}{\pi r_\mathrm{n} \beta_{g'}^2 J_0^2\left(\beta_{g'}\right) \cosh\left(\beta_{g'} l_\mathrm{m}/r_\mathrm{m}\right)} \tag{S4}$$

where the subscript 'm' indicates that we are considering the solution only in the macroscopic exterior compartment, $-\left(2l_\mathrm{m} + l_\mathrm{n}\right)/2 \leq z \leq -l_\mathrm{n}/2$.

We now consider the solution for the potential in the bottom half of the nanochannel. The electric potential is again antisymmetric, $\phi\,(r,\ -z) = -\phi\,(r,\ z)$, so that

$$\phi_\mathrm{n}\,(r,\ 0) = 0 \tag{S5}$$

where the subscript 'n' indicates that we are considering the solution only in the bottom half of the nanochannel,

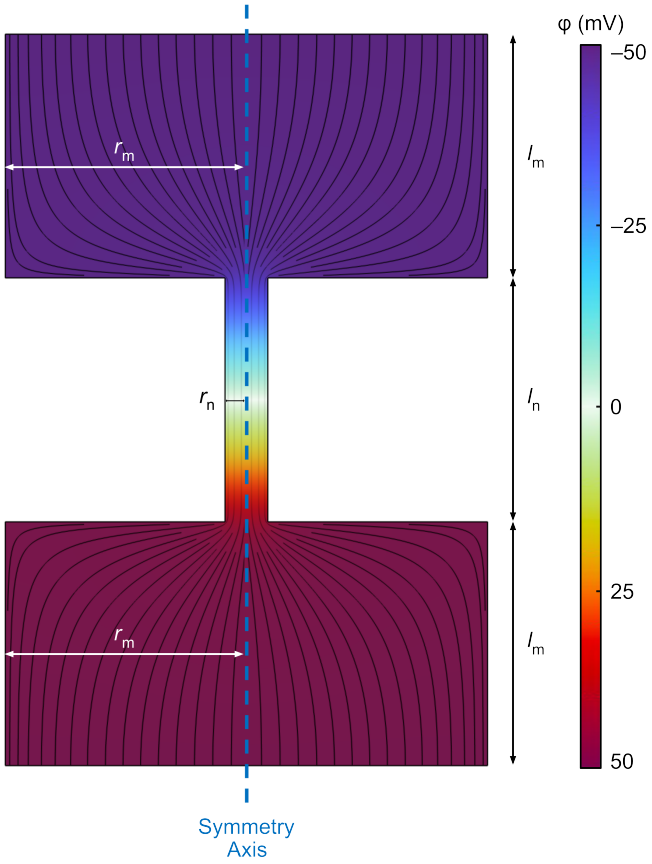

FIG. S1. The single nanochannel geometry. The nanochannel has radius r_n and length l_n and is connected at both ends to an exterior macroscopic compartment of radius r_m and length l_m. The top side of the system is held at $-\frac{\Delta V}{2}$, and the bottom side of the system is held at $\frac{\Delta V}{2}$. Equipotential false coloring and current streamlines extracted from finite element method simulations are also shown.

$-l_\mathrm{n}/2 \leq z \leq 0$. Additionally, we require no flux of the electric potential through the compartment walls so that

$$\left.\frac{\partial \phi_\mathrm{n}}{\partial r}\right|_{r=r_\mathrm{n}} = 0 \tag{S6}$$

from which we obtain $k_{g,\mathrm{n}} = \beta_g / r_\mathrm{n}$ and $A_\mathrm{n} = 0$. At $z = -l_\mathrm{n}/2$, as for the case with two pores in series, we have

$$\left.\frac{\partial \phi_\mathrm{n}}{\partial z}\right|_{z=-l_\mathrm{n}/2} = -\rho_\mathrm{bulk} i\,(r) \tag{S7}$$

Using the assumption of a radial inverse square root current density, we therefore obtain in the same manner as

before

$$B_{\rm n} = -\rho_{\rm bulk}\frac{I}{\pi r_{\rm n}^2} \tag{S8}$$

and

$$a_{g',{\rm n}} = -\frac{\rho_{\rm bulk} I \sin\left(\beta_{g'}\right)}{\pi r_{\rm n}\beta_{g'}^2 J_0^2\left(\beta_{g'}\right)\cosh\left(\beta_{g'} l_{\rm n}/2r_{\rm n}\right)} \tag{S9}$$

We now have the solution for the electric potential in both compartments. Matching the solutions for these two compartments at the boundary between the nanochannel and the exterior compartment, we arrive at the expression for the resistance of the entire system

$$R = \Delta V/I = R_{\rm bulk} + 2R_{\rm f,n} + 2R_{\rm a,m} \tag{S10}$$

where the bulk resistance term is given by

$$R_{\rm bulk} = \frac{\rho_{\rm bulk} l_{\rm n}}{\pi r_{\rm n}^2} + 2\frac{\rho_{\rm bulk} l_{\rm m}}{\pi r_{\rm m}^2} \tag{S11}$$

and the access resistance $R_{\rm a,m}$, which arises on both sides of the nannochannel, is given by

$$R_{\rm a,m} = \sum_{g=1}^{\infty} \frac{\rho_{\rm bulk}\sin\left(\beta_g r_{\rm n}/r_{\rm m}\right)\tanh\left(\beta_g l_{\rm m}/r_{\rm m}\right)}{\pi r_{\rm n}\beta_g^2 J_0^2\left(\beta_g\right)} \tag{S12}$$

We also have two times an additional term, $R_{\rm f,n}$, which corresponds to the redistribution of the current density from the mouth of the nanochannel to its center, and is given by the expression

$$R_{\rm f,n} = \sum_{g=1}^{\infty} \frac{\rho_{\rm bulk}\sin\left(\beta_g\right)\tanh\left(\beta_g l_{\rm n}/2r_{\rm n}\right)}{\pi r_{\rm n}\beta_g^2 J_0^2\left(\beta_g\right)} \tag{S13}$$

We may also solve for the resistance of the system assuming a constant current density. The calculation proceeds in exactly the same was as for the case with the radial inverse square root current density but with $i(r)$ given by Eq. (10) in the main text instead of Eq. (11). The coefficients remain exactly the same with the exception of

$$a_{g',{\rm m,\ const}} = -\frac{2\rho_{\rm bulk} I J_1\left(\beta_{g'} r_{\rm n}/r_{\rm m}\right)}{\pi r_{\rm n}\beta_{g'}^2 J_0^2\left(\beta_{g'}\right)\cosh\left(\beta_{g'} l_{\rm m}/r_{\rm m}\right)} \tag{S14}$$

and

$$a_{g',{\rm n,\ const}} = 0 \tag{S15}$$

Matching the solutions at the boundary gives

$$R_{\rm const} = \Delta V/I = R_{\rm bulk} + 2R_{\rm a,m,const} \tag{S16}$$

where the bulk resistance term is again given by Eq. (S11) and the access resistance $R_{\rm a,m}$, which arises on both sides of the nanochannel, is given by

$$R_{\rm a,m,const} = \sum_{g=1}^{\infty} \frac{2\rho_{\rm bulk} J_1\left(\beta_g r_{\rm n}/r_{\rm m}\right)\tanh\left(\beta_g l_{\rm m}/r_{\rm m}\right)}{\pi r_{\rm n}\beta_g^2 J_0^2\left(\beta_g\right)} \tag{S17}$$

With the assumption of a uniform current density in the nanochannel, we therefore recover the simple expression for the total resistance as the sum of the bulk resistance and the access resistance at the two ends of the channel without the additional term that was found for the case of a radial inverse square root current density.

For small $l_{\rm n}$, we expect the radial inverse square root current density model to better describe the system. As $l_{\rm n}$ increases, the current density at the mouth of the pore is expected to become more uniform, leading to significant deviation from the predictions of the radial inverse square root current density model and an increase in the access resistance towards the predicted value from the uniform current density model. However, even for very large $l_{\rm n}$, it is expected that a uniform current density will only develop far from the mouth of the pore so that the access resistance will never actually reach the predicted value of the uniform current density model.[1] It is expected expected that both the radial inverse square root current density model and the uniform current density model will fail to provide an accurate description of the access resistance of the system for large values of $l_{\rm n}$. It is important to note, however, that for these large values of $l_{\rm n}$, the contribution to the total resistance from the access resistance becomes negligible compared to that of the bulk resistance and the exact form of the access resistance no longer matters in determining the total resistance of the system.

In order to test these predictions of the validity of these single channel models, we conducted finite element method simulations for single nanochannel geometries. Fig. S2a shows the current density in the middle of the channel normalized by $I/\pi r_{\rm n}^2$ for different values of $l_{\rm n}/r_{\rm n}$. As expected, the current density approaches the form of Eq. (10) in the main text for large $l_{\rm n}$. Fig. S2b shows

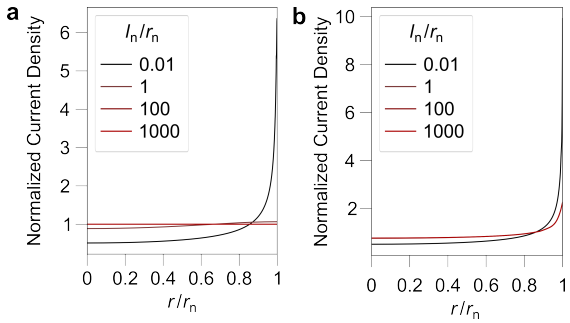

FIG. S2. The current density normalized by $I/\pi r_{\rm n}^2$ for various $l_{\rm n}/r_{\rm n}$ at (a) the middle of the nanochannel and (b) the mouth of the nanochannel.

the current density at the mouth of the channel normalized by $I/\pi r_{\rm n}^2$ for different values of $l_{\rm n}/r_{\rm n}$. Unlike the current density at the center of the channel, the current density at the mouth of the channel does not approach a uniform current density for large values of $l_{\rm n}$. Consequently, as shown in Fig. S3, which shows the values of the access resistance as a function of $l_{\rm n}/r_{\rm n}$, the val-

ues start out in agreement with the radial inverse square root current density model and increase towards those predicted assuming a uniform current density. However, well before reaching the predicted value using a uniform current density, the value of the access resistance saturates. Interestingly, the value at which the access resistance saturates is approximately 1.05 times the value predicted for a nanochannel of negligible length, comparable to the Maxwell-Rayleigh correction to the access resistance for a cylindrical conductor in contact with a semi-infinite conductor.[1]

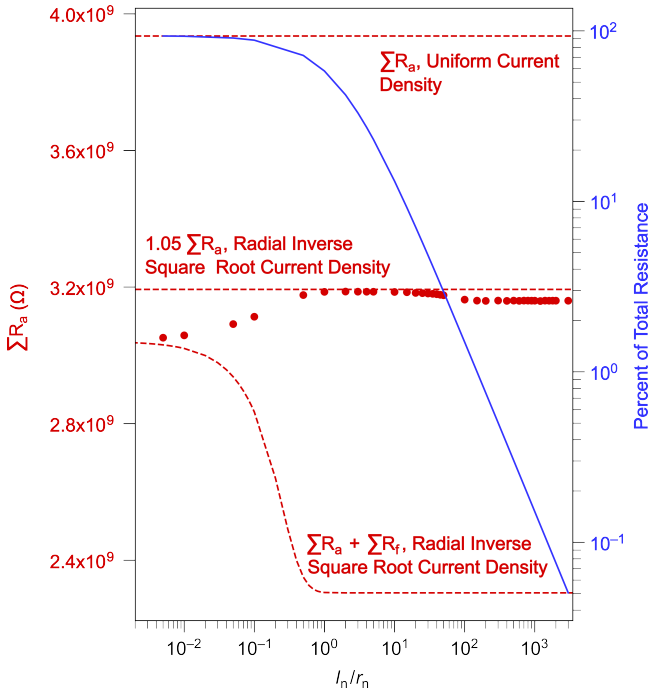

FIG. S3. The total access resistance as a function of l_n/r_n for the case of a single nanochannel. The predicted access resistance for the model assuming a uniform current density, the model using the radial inverse square root current density, and 1.05 times the prediction for the access resistance assuming a radial inverse square root density and a pore of negligible thickness are plotted as dashed lines. In blue, the percentage of the total resistance that the access resistance contributes is plotted as a function of l_n/r_n.

In Fig. S3 we also plot the percent fraction of the total resistance contributed by the access resistance (blue solid line, right y axis). For $l_n \gtrsim 150\ r_n$, the access resistance contribution to the total resistance becomes negligible ($< 1\%$). The accurate extraction of the access resistance from simulations of systems with longer pore lengths becomes challenging, as the contribution from the access resistance then becomes increasingly comparable to the error of the numerical solution itself. However, for these values, it is clear that the exact form of the access resistance is no longer important in determining the total resistance of the system.

S2. EFFECTS OF FINITE THICKNESS OF THE PORES

The analytical model considers the case where the thickness of the pores is negligible. However, for real systems, obviously the pores must have a finite thickness. The finite element method simulations required that the nanopores have a finite thickness, which was generally chosen to be two or three orders of magnitude smaller than the radius of the pores, and therefore the simulation results verify that the model is valid as long as $l_n \ll 2r_n$.

For the very relevant case where the radius of the pores becomes comparable to the thickness of the pores, the contribution from the bulk resistance of the pores is expected to become important, particularly when $l_n \gtrsim r_n/4$. Simulations were carried out for these cases, and we find that the model still works well as long as the bulk resistance of the nanopores is included. As was done for the case of negligible nanopore thickness, the total access resistance, $\sum R_a = 2R_{a,c} + 2R_{a,m}$, was obtained from the simulation data by subtracting the bulk resistance from the total resistance of the system where the bulk resistance is now given by

$$R_{bulk} = \frac{\rho_{bulk} l_c}{\pi r_c^2} + 2\frac{\rho_{bulk} l_m}{\pi r_m^2} + 2\frac{\rho_{bulk} l_n}{\pi r_n^2} \qquad \text{(S18)}$$

to account for the contribution from the two nanopores. In Fig. S4, the total access resistance as a function of the central channel length ranging from 2 nm to 200 nm is plotted for r_n/r_c ratios of 0.025, 0.05, and 0.1 and nanopore thicknesses, l_n, of 0.34 nm, 1.0 nm, 1.5 nm, and 2.0 nm. The total access resistances computed from Eq. (24) and Eq. (25) are shown by the solid lines in the figure. The deviation of the total access resistance from the results for $l_n \ll 2r_n$ remains less than 5% in all cases. The deviation from the predictions of the analytical model remains less than 5% in most cases as well, except for when l_c approaches l_n for which the deviation reached up to 13.5%. This result is expected, as, for these ratios of r_n/r_c, the system falls within the coupling regime where the access resistance was found to be higher than that predicted by the model due to the variation in the current density from the approximate form, and, as the length of the pores is increased, the current density also becomes more uniform resulting in an increase in the access resistance as well, so the effects are additive and result in greater deviations from the predictions of the model.

S3. EFFECTS OF SURFACE CHARGE

To examine the effects of surface charge, additional simulations were performed where the membrane surfaces were assigned a surface charge density of σ while the outer surfaces of the reservoirs and central channel were assigned a surface charge density of zero. Again,

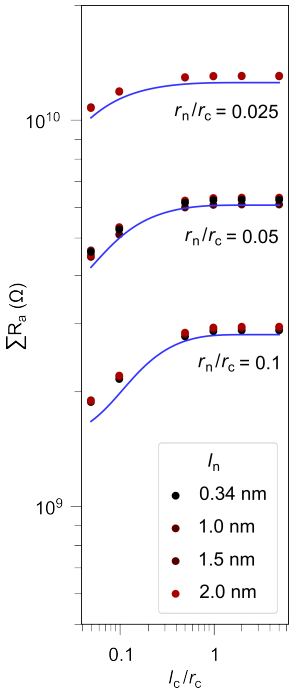

FIG. S4. The total access resistance, $\sum R_a$, as a function of l_c/r_c for various ratios of r_n/r_c and different thicknesses of the nanopores, l_n. The solid lines show the values for the total access resistance given by the analytical model.

a voltage difference of $\Delta V = 0.1$ V was chosen for the simulations so that the top of the system was held at 0.05 V and the bottom was held at −0.05 V. The required finite length of the nanopores was chosen so that $l_n/2r_n \ll 1$. The outer walls of the channels were set to satisfy $\vec{J}_\pm \cdot \vec{n} = 0$, where again $\vec{J}_\pm$ represents the fluxes of the positive and negative ion species and $\vec{n}$ is the unit vector normal to the channel walls. The charge numbers of the two ion species were chosen to be $z_\pm = \pm 1$. The length of the exterior compartments was set equal to their radius, $r_m = l_m$, and values for l_m were chosen that are much larger than the nanopore radius r_n as well as the Debeye length, $l_D = \sqrt{\varepsilon k_B T/2z^2e^2C}$, which characterizes the thickness of the electric double layer (EDL) formed at the charged surface of the membrane.[2] At this distance, the local concentration approaches the bulk, so that c_+, $c_- = C$ at both ends of the system. Due to the surface charge, a charge density could arise within the fluid given by $\rho = e(c_+ - c_-)$. In order to ensure that our simulations accurately captured the effect of the EDL, we set the mesh size of our model to be much smaller than l_D and the Gouy-Chapman length, $l_{GC} = 2\varepsilon k_B T/|\sigma|e$, close to the charged boundaries.[3] These simulations were also governed by Poisson's equation

$$\nabla^2\phi = -\frac{\rho}{\varepsilon} \tag{S19}$$

and the steady state Nernst-Planck equation

$$\vec{J}_\pm = -D_\pm(\vec{\nabla}c_\pm \pm \frac{e}{k_B T}c_\pm\vec{\nabla}\phi) \tag{S20}$$

As was done for the case of zero surface charge on the nanopores, values of $D_\pm = 1.0 \times 10^{-9}$ m^2/s for the ion diffusivities, $T = 293.15$ K for the temperature, and $\varepsilon_r = 80$ for the relative permittivity of the electrolyte solution were used for the simulations. A range of concentrations from 0.5 mol/m^3 to 3000 mol/m^3 were used as well as a range of negative surface charge densities from −0.00001 C/m^2 to −1.0 C/m^2 in order to characterize when our purely geometrical analytical model can be expected to break down. The results indicate that the proper length scale to characterize the breakdown of the geometric model is the Dukhin length as calculated using the expression[3]

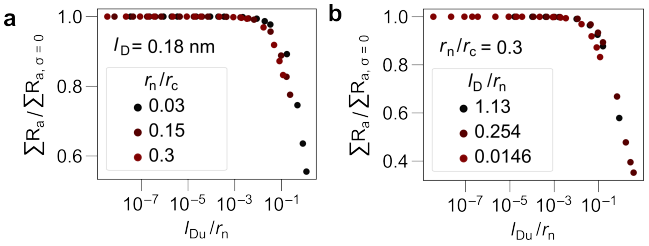

FIG. S5. The total access resistance, $\sum R_a$, normalized by the total access resistance with zero surface charge on the nanopores, $\sum R_{a,\,\sigma=0}$, as a function of l_{Du}/r_n for (a) various ratios of r_n/r_c and constant l_D and (b) various ratios of l_D/r_n and constant r_n/r_c.

$$l_{Du} = \frac{|\sigma|}{2eC}\left[-\frac{l_{GC}}{l_D} + \sqrt{\frac{l_{GC}^2}{l_D^2} + 1}\right] \tag{S21}$$

and normalized by the radius of the nanopore, l_{Du}/r_n. Fig. S5a shows the total access resistance, $\sum R_a$, normalized by the total access resistance with zero surface charge on the nanopores, $\sum R_{a,\,\sigma=0}$, as a function of l_{Du}/r_n for various ratios of r_n/r_c and constant $l_D = 0.18$ nm. Fig. S5b shows the total access resistance, $\sum R_a$, normalized by the total access resistance with zero surface charge on the nanopores, $\sum R_{a,\,\sigma=0}$, as a function of l_{Du}/r_n for various ratios of l_D/r_n and constant $r_n/r_c = 0.3$. Regardless of the size of the nanopore or the size of the Debye length in comparison to the size of the pore, significant deviation from the results for no surface charge (greater than $\sim 5\%$) occurs at $\sim 0.05r_n$. Using this guideline, the surface charge density or the concentration at which the model breaks down can easily be obtained.

S4. CONVERGENCE OF THE BESSEL SERIES

The expressions for the access resistance that have been derived involve infinite sums of Bessel functions of the form

$$R_{\rm a} = \sum_{g=1}^{\infty} \frac{\rho_{\rm bulk} \sin\left(\beta_g r_{\rm n}/r_{\rm m}\right) \tanh\left(\beta_g l_{\rm m}/r_{\rm m}\right)}{\pi r_{\rm n} \beta_g^2 J_0^2\left(\beta_g\right)} \tag{S22}$$

To quickly evaluate sums of this form, we consider the asymptotic limit of β_g, $\beta_g \approx \pi(g+1/4) \approx \pi g$ and the fact that, for $x \to \infty$, $J_0(x) \to \sqrt{\frac{2}{\pi x}} \cos\left(x - \frac{\pi}{4}\right)$.[4] For large g, we therefore have $\beta_g^2 J_0^2(\beta_g) \approx 2(g+1/4)$. For large β_g, we may also set $\tanh\left(\beta_g \frac{l_{\rm m}}{r_{\rm m}}\right) \approx 1$. Therefore, for large g, we have

$$R_{\rm a}^{\rm asymptotic} = \frac{\rho_{\rm bulk}}{\pi r_{\rm n}} \sum_{g=1}^{\infty} \frac{\sin\left(\pi\left(g+\frac{1}{4}\right)\frac{r_{\rm n}}{r_{\rm m}}\right)}{2\left(g+\frac{1}{4}\right)} \tag{S23}$$

which has a closed form solution that is quickly evaluated,

$$R_{\rm a}^{\rm asymptotic} = \frac{\rho_{\rm bulk}}{\pi r_{\rm n}} \left[e^{i\frac{\pi r_{\rm n}}{4 r_{\rm m}}} - {}_2F_1\left(\frac{1}{4}, 1; \frac{5}{4}; e^{i\pi\frac{r_{\rm n}}{r_{\rm m}}}\right) - ie^{-i\frac{\pi r_{\rm n}}{4 r_{\rm m}}} + i\ {}_2F_1\left(\frac{1}{4}, 1; \frac{5}{4}; e^{-i\pi\frac{r_{\rm n}}{r_{\rm m}}}\right)\right] \tag{S24}$$

where ${}_2F_1\left(a, b; c; z\right)$ is the hypergeometric function. We now correct the expression for the first $g_{\rm cutoff}$ terms,

$$R_{\rm a} = R_{\rm a}^{\rm asymptotic} + \frac{\rho_{\rm bulk}}{\pi r_{\rm n}} \left[\sum_{g=1}^{g_{\rm cutoff}} \frac{\sin\left(\beta_g r_{\rm n}/r_{\rm m}\right) \tanh\left(\beta_g l_{\rm m}/r_{\rm m}\right)}{\beta_g^2 J_0^2\left(\beta_g\right)} - \sum_{g=1}^{g_{\rm cutoff}} \frac{\sin\left(\pi\left(g+\frac{1}{4}\right)\frac{r_{\rm n}}{r_{\rm m}}\right)}{2\left(g+\frac{1}{4}\right)} \right] \tag{S25}$$

A reasonable choice for the cutoff is $g_{\rm cutoff} = \max\left(2\frac{r_{\rm m}}{r_{\rm n}}, 2\frac{r_{\rm m}}{l_{\rm m}}\right)$. The first argument of $g_{\rm cutoff}$ ensures the sine term is properly evaluated for arguments up to at least 2π. The second argument of $g_{\rm cutoff}$ ensures that the tanh term is properly evaluated for arguments up to at least 2π. Note that $\tanh\left(2\pi\right) = 0.999993$, and that the tanh term may be safely approximated by 1 for larger arguments. We list the $g_{\rm cutoff}$ needed to achieve convergence better than 0.1% for select ratios $r_{\rm n}/r_{\rm m}$ and $l_{\rm m}/r_{\rm m}$ in Table S4.

$r_{\rm n}/r_{\rm m}$ \ $l_{\rm m}/r_{\rm m}$	0.01	0.1	1	10	100
0.0001	28	1	1	1	1
0.001	66	3	1	1	1
0.01	76	6	1	1	1
0.1	101	7	5	5	5

TABLE S1. Values of $g_{\rm cutoff}$ needed for convergence to within 0.1%.

REFERENCES

[1] R. Holm, *Electric contacts: theory and application*, 4th ed. (Springer-Verlag, Berlin Heidelberg, Germany, 1967).

[2] L. Bocquet and E. Charlaix, "Nanofluidics, from bulk to interfaces," Chem. Soc. Rev. **39**, 1073–1095 (2010).

[3] C. Lee, L. Joly, A. Siria, A.-L. Biance, R. Fulcrand, and L. Bocquet, "Large apparent electric size of solid-state nanopores due to spatially extended surface conduction," Nano Lett. **12**, 4037–4044 (2012).

[4] A. Gray and G. B. Mathews, *A treatise on Bessel functions and their applications to physics* (Macmillan and Co., London, UK, 1895).